Magnetisation processes, hysteresis and finite-size effects in model multilayer systems of cubic or uniaxial anisotropy with antiferromagnetic coupling between adjacent ferromagnetic layers

Magnetisation processes, hysteresis and finite-size effects in model multilayer systems of cubic or uniaxial anisotropy with antiferromagnetic coupling between adjacent ferromagnetic layers

B Dieny†, J P Gavigan and J P Rebouillat

Laboratoire Louis Néel, CNRS, 166 X, 38042 Grenoble Cédex, France

Abstract. Magnetisation processes have been investigated for model multilayer systems where antiferromagnetic interactions couple adjacent ferromagnetic layers. In this first study, only coherent rotations of the magnetisation of each layer are taken into account. Depending on the direction of the applied magnetic field, the initial moment configuration and the magneto-crystalline anisotropy, various first- or second-order magnetic transitions may be observed.

The cases of cubic and uniaxial anisotropy bilayer systems are treated in detail. Spin-flop and spin-flip transitions are calculated to occur for both symmetries when starting from antiferromagnetic configurations that are parallel to the field axis. In the cubic case, various other transitions have been found. In particular, first-order transitions between symmetric and non-symmetric states have been calculated, involving asymmetric behaviour of the magnetisation vectors of adjacent layers. Such transitions give rise to a transverse magnetisation. All the critical transition fields have been calculated as a function of the anisotropy and are reported in the various phase diagrams.

Hysteresis loops have also been calculated. They generally consist of an upper and a lower part shifted symmetrically about the origin as in the case of bulk antiferromagnets.

The influence of the number of layers has been investigated in some particular cases. It is shown that in most instances when the number of layers n becomes very large (i.e. when boundary effects disappear), the multilayer behaves like a bilayer but with different transition-field values. For small numbers of layers, whether or not the magnetism is compensated (n even or odd) has a very strong effect on the magnetisation processes.

1. Introduction

The synthesis of artificially layered materials has attracted much attention over the last decade. Studies of novel heterostructures tailored on length scales characteristic of important physical interactions have led to the discovery of many new physical properties (for a review, see [1]). In the case of magnetic superlattices, most studies have focused on the magnetic behaviour of thin layers and interfaces. Some studies, however, have focused on long-range and collective phenomena representative of the superlattice as a whole [2, 3]. Inter-planar magnetic coupling through non-magnetic layers has been

---

† Present address: IBM Almadeu Research Center, 650 Harry Road, K63/803 San Jose, CA 95120-6099, USA

observed for various modulated compositions (for a review, see [4]), such as Cu/Ni, Mo/Ni [5], Fe/V [6], Co/Cr [7], Fe/Cu [8] and Dy/Y [9], giving rise to ferromagnetic, antiferromagnetic or helicoidal superstructures as well as modifications in the spin-wave mode spectra [8]. Several mechanisms have been proposed for this coupling, including dipolar and Ruderman–Kittel–Kasuya–Yosida (RKKY) interactions as well as per-colation phenomena. It seems, however, that a certain amount of conjecture and contention remains as to what the actual mechanism(s) may be.

In this paper we report a phenomenological study, at zero temperature, of the magnetic behaviour of model multilayer systems of cubic and uniaxial in-plane ani-sotropy with assumed antiferromagnetic coupling between adjacent identical ferro-magnetic layers (e.g. $(0\,0\,1)$Fe/$(0\,0\,1)$Cr BCC [10], Co/Cu [11]). Such a study does not demand any assumption regarding the microscopic nature of the magnetic coupling. Calculation of the field and anisotropy dependences of magnetic structure yields initial magnetisation curves, hysteresis loops and magnetic phase diagrams for the model systems. In general, magnetisation processes in a magnetic material involve the nucleation of domains with domain-wall propagation and/or coherent rotation of the magnetisation. The tendency towards one or other mechanism depends on the domain-wall energy and on their pinning. In this first study, we focus on the magnetisation processes that occur through coherent rotation of the magnetisation. In a following paper, we shall consider the other limiting behaviour of the pure non-dissipative nucleation–propagation mechanism and compare with hysteresis loops measured for real multilayers. Thus, we assume here that each ferromagnetic layer is single-domain and that its magnetisation rotates as a rigidly coupled block of moments. Moreover, it is assumed that strong shape and/or negative perpendicular anisotropy confines the magnetic moments of the sublayers to the film plane. These assumptions correspond, for instance, to the situation in Fe/Cr multilayers with $[1\,0\,0]$ type growth [12].

Based on the above assumptions, the magnetic superlattice may be modelled as a one-dimensional system of n moments $M_1, \ldots, M_n$ of the same rigid modulus. In calculating the in-plane magnetisation process, these moments are described by the angles $(\theta_1, \ldots, \theta_n)$ that they make with the direction of the applied field. The internal energy is written as

$$E = J_0(M_1 . M_2 + \ldots + M_{i-1} . M_i + M_i . M_{i+1} + \ldots + M_{n-1} . M_n) - (M_1 + \ldots$$
$$+ M_i + \ldots + M_n) . B + (E_{A1} + \ldots + E_{Ai} + \ldots + E_{An}) \qquad (1)$$

where J_0 represents the antiferromagnetic coupling ($J_0 > 0$) between adjacent layers, B is the applied field and E_{Ai} is the anisotropy energy of the ith layer. E_{Ai} is given by $-D \cos^2 \theta_i$ for the uniaxial case and by $K \cos^2 \theta_i \sin^2 \theta_i$ for the cubic case, with D and $K > 0$ (<0) for B applied along an easy (hard) magnetisation direction. In order to calculate the magnetisation curves, we minimise the energy using the steepest-descent method. For simplicity, all magnetic-moment and magnetisation vectors are assumed to have unit modulus. The equilibrium positions are given by the set of n coupled equations $(\partial E/\partial \theta_i) = 0$ $(i = 1$ to $n)$

$$-J_0 \sin(\theta_1 - \theta_2) + B \sin \theta_1 + \partial E_{A1}/\partial \theta_1 = 0$$
$$\vdots$$
$$-J_0 \sin(\theta_i - \theta_{i+1}) - J_0 \sin(\theta_i - \theta_{i-1}) + B \sin \theta_i + \partial E_{Ai}/\partial \theta_i = 0 \qquad (2)$$
$$\vdots$$
$$-J_0 \sin(\theta_n - \theta_{n-1}) + B \sin \theta_n + \partial E_{An}/\partial \theta_n = 0$$

with the stability condition that all the eigenvalues of the matrix M defined by

$$M_{ij} = (\partial^2 E/\partial\theta_i\partial\theta_j)$$

should be positive. This condition gives rise to critical lines in the (D, B) or (K, B) planes corresponding to the appearance of a path on the energy surface $E(\theta_1 \ldots \theta_n)$ which permits the system to slide from its current unstable state into the most accessible minimum. The crossing of these critical lines is manifested by first- or second-order magnetic transitions.

In the following sections (§§ 2 and 3), we shall focus on the case of a bilayer. Although it represents a limited case, it contains most of the physics of the magnetisation processes for such systems.

Taking only two variables θ_1 and θ_2, the set of equations (2) reduces to

$$-J_0 \sin(\theta_1 - \theta_2) + B \sin\theta_1 + \partial E_{A1}/\partial\theta_1 = 0$$
$$-J_0 \sin(\theta_2 - \theta_1) + B \sin\theta_2 + \partial E_{A2}/\partial\theta_2 = 0$$

$$(3a)$$

and the stability condition becomes

$$\frac{\partial^2 E}{\partial\theta_1^2} \times \frac{\partial^2 E}{\partial\theta_2^2} - \left(\frac{\partial^2 E}{\partial\theta_1\partial\theta_2}\right)^2 > 0. \tag{3b}$$

In what follows, the anisotropy constants, D or K, and magnetic field B are normalised to the strength of the antiferromagnetic coupling J_0 and the notation d, k and b is used.

In § 4, we shall investigate for a number of cases the influence of the number of layers on the magnetisation processes.

2. Magnetisation and demagnetisation processes for cubic in-plane anisotropy

2.1. Zero-field configurations and low-field susceptibilities

The cubic anisotropy energy is given by $E_A = k \cos^2\theta \sin^2\theta$, so that when $k > 0$, $(1\,0\,0)$ or $(0\,1\,0)$ are the easy axes of magnetisation while they are $(1\,1\,0)$ or $(\bar{1}\,1\,0)$ for $k < 0$. Magnetisation and demagnetisation processes will be examined for both cases. The set of equations (3) giving the equilibrium positions of the two moments and stability become for cubic anisotropy

$$\partial E/\partial\theta_1 = -\sin(\theta_1 - \theta_2) + b \sin\theta_1 + (k/2)\sin(4\theta_1) = 0$$
$$\partial E/\partial\theta_2 = +\sin(\theta_1 - \theta_2) + b \sin\theta_2 + (k/2)\sin(4\theta_2) = 0$$

$$(4a)$$

and

$$-2\cos(\theta_1 - \theta_2) + b(\cos\theta_1 + \cos\theta_2) + 2k[\cos(4\theta_1) + \cos(4\theta_2)] > 0$$
$$\times [-\cos(\theta_1 - \theta_2) + b \cos\theta_1 + 2k \cos(4\theta_1)][-\cos(\theta_1 - \theta_2)$$
$$+ b \cos\theta_2 + 2k \cos(4\theta_2)] - \cos^2(\theta_1 - \theta_2) > 0. \tag{4b}$$

The system of coupled equations for zero field reduce to

$$(k/2)\sin(4\theta_1^0) - \sin(\theta_1^0 - \theta_2^0) = 0$$
$$(k/2)\sin(4\theta_2^0) + \sin(\theta_1^0 - \theta_2^0) = 0$$

$$(5)$$

where the solutions (θ_1^0, θ_2^0) represent the zero-field moment configurations. One, two or three types of solution can be found depending on the strength of the anisotropy.

In order to classify the different possible states, the following notation is used. Fourth-order cubic anisotropy gives rise to four wells of energy positioned with respect to the crystallographic axes at [1 0], [0 1], [$\bar{1}$ 0] and [0 $\bar{1}$] ([1 1], [1 $\bar{1}$], [$\bar{1}$ $\bar{1}$] and [$\bar{1}$ 1]) for $k > 0$ (<0). A third index is not used as only in-plane magnetisation processes are considered. The position of a magnetic moment is conveniently labelled according to the well of energy in which it lies. Therefore, four indices are needed to characterise any initial state (two moments), as will be illustrated in discussing each type of solution. Note that the field is always taken to point along the [1 0] direction.

Type I: antiparallel states $(\theta_1^0 = \theta_2^0 - \pi)$. Such states exist for all values of k. The general solutions of equations (5) are given by $\theta_1^0 = 0 + m\pi/2 = \theta_2^0 - \pi$ for $k > 0$ and $\theta_1^0 = \pi/4 + m\pi/2 = \theta_2^0 - \pi$ for $k < 0$. The inequivalent states with respect to the applied field are labelled [1 0, $\bar{1}$ 0], [0 1, 0 $\bar{1}$] for $k > 0$ and [1 1, 1 $\bar{1}$] for $k < 0$ (see figure 1).

Type II: quasi-perpendicular states $(\theta_1^0 + \varepsilon = \theta_2^0 - (\pi/2 + \varepsilon))$. In this case, the moments occupy adjacent wells of energy with the antiferromagnetic coupling causing a symmetric relative canting of 2ε out of the purely perpendicular configuration. The solutions are therefore $\theta_1^0 = -\varepsilon + m\pi/2$, $\theta_2^0 = \pi/2 + \varepsilon + m\pi/2$ for $k > 0$ and $\theta_1^0 = -\varepsilon + \pi/4 + m\pi/2$, $\theta_2^0 = 3\pi/4 + \varepsilon + m\pi/2$ for $k < 0$. Substituting into (5) leads to the equation
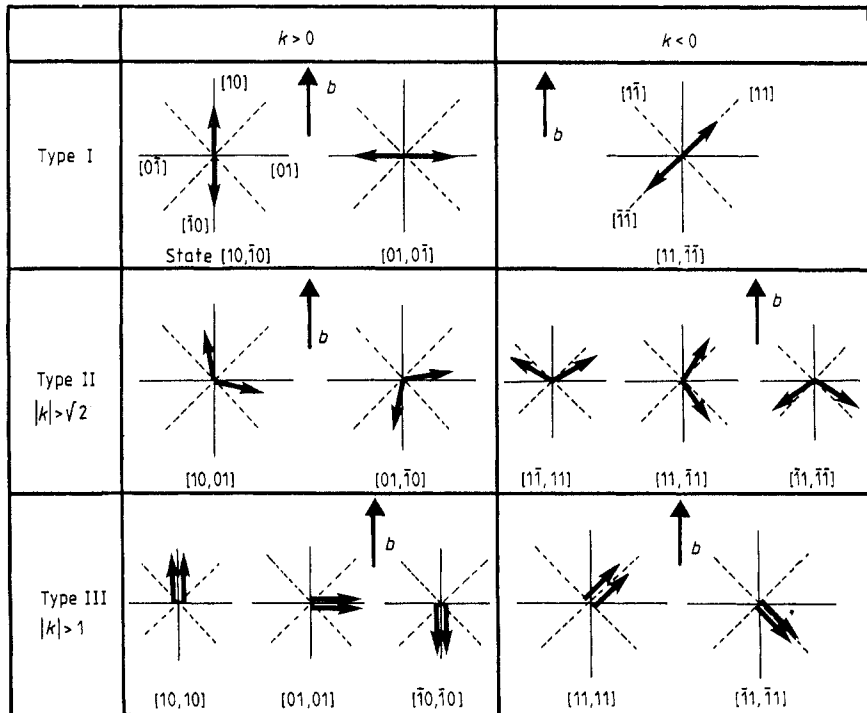
$$\varepsilon = \tfrac{1}{2}\sin^{-1}|1/k|. \tag{6}$$

Figure 1. Schematic representation of the possible initial moment configurations for both positive and negative cubic anisotropy.

The inequivalent states with respect to the field are labelled $[1\,0, 0\,1]$, $[\bar{1}\,0, 0\,1]$ for $k > 0$ and $[1\,\bar{1}, 1\,1]$, $[\bar{1}\,1, 1\,1]$, $[\bar{1}\,\bar{1}, \bar{1}\,1]$ for $k < 0$ (figure 1). It may be deduced from the stability condition in equations (4) that type II states are only stable when $|k| > \sqrt{2}$.

Type III: parallel states $(\theta_1^0 = \theta_2^0)$. In this case the solutions of equations (5) are $\theta_1^0 = \theta_2^0 = 0 + m\pi/2$ for $k > 0$ and $\theta_1^0 = \theta_2^0 = \pi/4 + m\pi/2$ for $k < 0$. The states of interest sketched in figure 1 are $[1\,0, 1\,0]$, $[0\,1, 0\,1]$, $[\bar{1}\,0, \bar{1}\,0]$ for $k > 0$ and $[1\,1, 1\,1]$, $[\bar{1}\,1, \bar{1}\,1]$ for $k < 0$. Similar to type II states, it may be deduced from equations (4) that these parallel states are only stable when $|k| > 1$.

Of all these different equilibrium states, therefore, those of type I with zero magnetisation are the most stable. Those of types II and III are metastable and of non-zero remanent magnetisation, which gives rise to the stability condition placed on the anisotropy. At first sight, it may be surprising that there is a more stringent anisotropy requirement to stabilise type II rather than type III states. However, the repulsive torque that the moments exert on each other is proportional to $\sin(\theta_1 - \theta_2)$, and is therefore zero for type III states $(\theta_1 = \theta_2)$ and maximum when $\theta_1 - \theta_2 = \pi/2$, which is approximately the case for type II states. Values of the remanent magnetisation $|M_R^0|$ as well as parallel and transverse components $(M_{R\parallel}^0, M_{R\perp}^0)$ are reported for all the states in table 1.

Next, we consider what happens when we turn on a small magnetic field, and in particular what are the low-field parallel $(\chi_\parallel^0)$ and transverse $(\chi_\perp^0)$ susceptibilities. In such an instance, the 'field' terms in equations (4) remain and solutions of the type $\theta_1 = \theta_1^0 + \varepsilon_1$, $\theta_2 = \theta_2^0 + \varepsilon_2$ can be considered, where θ_1^0, θ_2^0 are the zero-field solutions and $\varepsilon_1, \varepsilon_2$ are small changes in angle induced by the field, not to be confused with ε of equation (6). Substituting the above for θ_1 and θ_2 in equations (4), making small-angle approximations for terms in ε_1 and ε_2 and using equations (5), one arrives at the following:

$$\varepsilon_1[2k\cos(4\theta_1^0) - \cos(\theta_1^0 - \theta_2^0)] + \varepsilon_2\cos(\theta_1^0 - \theta_2^0) = -b\sin\theta_1^0$$
$$\varepsilon_1\cos(\theta_1^0 - \theta_2^0) + \varepsilon_2[2k\cos(4\theta_2^0) - \cos(\theta_1^0 - \theta_2^0)] = -b\sin\theta_2^0. \tag{7}$$

Solving (7) for ε_1/b and ε_2/b yields

$$-\varepsilon_1/b = [2k\sin\theta_1^0\cos(4\theta_2^0) - \cos(\theta_1^0 - \theta_2^0)(\sin\theta_1^0 + \sin\theta_2^0)]/\Delta$$
$$-\varepsilon_2/b = [2k\cos(4\theta_2^0)\sin\theta_2^0 - \cos(\theta_1^0 - \theta_2^0)(\sin\theta_1^0 + \sin\theta_2^0)]/\Delta \tag{8}$$

where

$$\Delta = 4k^2\cos(4\theta_1^0)\cos(4\theta_2^0) - 2k\cos(\theta_1^0 - \theta_2^0)[\cos(4\theta_1^0) + \cos(4\theta_2^0)].$$

Now

$$M_\parallel = \cos\theta_1 + \cos\theta_2$$
$$= \cos\theta_1^0 + \cos\theta_2^0 - \varepsilon_1\sin\theta_1^0 - \varepsilon_2\sin\theta_2^0$$
$$= M_{R\parallel}^0 - \varepsilon_1\sin\theta_1^0 - \varepsilon_2\sin\theta_2^0.$$

This implies that

$$\chi_\parallel^0 = -(\varepsilon_1/b)\sin\theta_1^0 - (\varepsilon_2/b)\sin\theta_2^0. \tag{9}$$

Table 1. Values of the zero-field magnetisation ($|M_R^0|$) as well as values of its components parallel ($M_{R\parallel}^0$) and perpendicular ($M_{R\perp}^0$) to the applied field [10] direction, for the different initial moment configurations in the case of cubic anisotropy. Also reported are calculated first-order expressions for the low-field parallel and perpendicular susceptibilities.

Type	State	θ_1^0	θ_2^0	$|M_R^0|$	$M_{R\parallel}^0$	$M_{R\perp}^0$	$\chi_\parallel^0$	$\chi_\perp^0$
I $(k>0)$	$[10,1\bar0]$	0	π	0	0	0	0	0
	$[01,0\bar1]$	$\pi/2$	$-\pi/2$	0	0	0	$1/(1+k)$	0
II $(k>\sqrt2)$	$[10,01]$	$-\varepsilon$	$\pi/2+\varepsilon$	$[2(1-1/k)]^{1/2}$	$[1-1/k]^{1/2}$	$[1-1/k]^{1/2}$	$(2k^2-2k-1)/[4(k^2-2)(k-1)]$	$(2k-3)/[4(k^2-2)(k-1)]$
	$[01,\bar10]$	$\pi/2-\varepsilon$	$\pi+\varepsilon$	$[2(1-1/k)]^{1/2}$	$-[1-1/k]^{1/2}$	$[1-1/k]^{1/2}$	$(2k^2-2k-1)/[4(k^2-2)(k-1)]$	$(-2k+3)/[4(k^2-2)(k-1)]$
III $(k>1)$	$[10,10]$	0	0	2	2	0	0	0
	$[01,01]$	$\pi/2$	$\pi/2$	2	0	2	$1/k$	0
	$[\bar10,\bar10]$	π	π	2	-2	0	0	0
I $(k<0)$	$[11,\bar1\bar1]$	$\pi/4$	$5\pi/4$	0	0	0	$-1/[2(k-1)]$	$1/[2(k-1)]$
II $(k<-\sqrt2)$	$[1\bar1,11]$	$-\pi/4-\varepsilon$	$\pi/4+\varepsilon$	$[2(1+1/k)]^{1/2}$	$[2(1+1/k)]^{1/2}$	0	$-1/[2(k+1)]$	0
	$[11,\bar11]$	$\pi/4-\varepsilon$	$3\pi/4+\varepsilon$	$[2(1+1/k)]^{1/2}$	0	$[2(1+1/k)]^{1/2}$	$-(k+1)/[2(k^2-2)]$	0
	$[\bar11,\bar11]$	$3\pi/4-\varepsilon$	$5\pi/4+\varepsilon$	$[2(1+1/k)]^{1/2}$	$-[2(1+1/k)]^{1/2}$	0	$-1/[2(k+1)]$	0
III $(k<-1)$	$[11,11]$	$\pi/4$	$\pi/4$	2	$\sqrt2$	$\sqrt2$	$-1/(2k)$	$1/(2k)$
	$[\bar11,\bar11]$	$3\pi/4$	$3\pi/4$	2	$-\sqrt2$	$\sqrt2$	$-1/(2k)$	$-1/(2k)$

Similarly

$$\chi_\perp^0 = (\varepsilon_1/b) \cos \theta_1^0 + (\varepsilon_2/b) \cos \theta_2^0. \tag{10}$$

It is thus possible to deduce the expressions for $\chi_\parallel^0$ and $\chi_\perp^0$ given in table 1 for each possible initial state, using equations (6) and (8)–(10).

2.2. $k > 0$

In the following eight subsections (§§ 2.2.1–2.2.8) we discuss the magnetisation processes and properties of hysteresis loops relevant to the case when the field is applied along an easy direction of magnetisation. Typical magnetisation curves are presented together with the magnetic phase diagrams for each of the possible initial states.

2.2.1. Initial state [1 0, $\overline{1}$ 0]. It is known from the study of bulk antiferromagnets that the application of a field along [1 0] to such a system provokes either a spin-flop transition ($\theta_2 = -\theta_1$) if the anisotropy is low or a spin-flip transition ($\theta_1 = \theta_2 = 0$) if the anisotropy
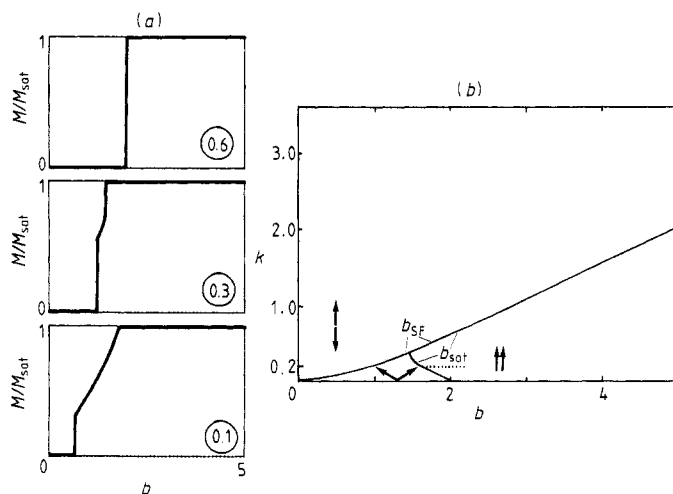
Figure 2. Initial state [1 0, $\overline{1}$ 0]. (*a*) Three typical magnetisation curves for the indicated anisotropy values $k = 0.1, 0.3$ and 0.6. (*b*) Phase diagram showing the critical lines associated with the spin-flop or spin-flip transition and with the reaching of saturation. The dotted line for $k = 0.2$ is the limit at which b_{sat} changes from a second-order to a first-order transition field. The arrows symbolise the moment orientations at the different stages of the magnetisation process.

is high. In figure 2(*a*) magnetisation curves calculated for different values of the anisotropy show such transitions, which define the line $b_{SF} = 2[k(k + 1)]^{1/2}$ in the magnetic phase diagram (figure 2(*b*)). For $k > 0.3740$, b_{SF} is a spin-flip transition field and is therefore equal to b_{sat} (the field at which the magnetisation reaches saturation). For $k < 0.3740$, $b_{SF} < b_{sat}$, and saturation can be reached by either a second-order transition when $k < 0.2$ or a first-order transition when $0.2 < k < 0.3740$. Expressions for b_{sat} for the different cases are summarised as follows:

$$b_{sat} = \begin{cases} 2(1 - k) & \text{if } k < 0.2 \\ \frac{4}{3}[(1 + k)^3/6k]^{1/2} & \text{if } 0.2 < k < 0.3740 \\ b_{SF} = 2[k(k + 1)]^{1/2} & \text{if } 0.3740 < k. \end{cases} \tag{11}$$

Note that after the spin-flop transition, the susceptibility is not constant and a positive curvature is observed in the corresponding magnetisation curve.

2.2.2. Initial state [0 1, 0 $\bar{1}$].

The two moments are initially transverse to the field. Here, also, three situations are encountered depending on the strength of the anisotropy, as illustrated by the magnetisation curves in figure 3(a). All curves are characterised by a finite low-field susceptibility $\chi_0 = 1/(1 + k)$ (table 1) with a small amount of positive curvature. For $k < 0.2$, the two moments remain symmetrical with respect to the applied field, closing to saturation at $b_{sat} = 2(1 - k)$ by a second-order transition as in the previous case. For intermediate anisotropy $0.2 < k < 0.5$, saturation is reached at a field $b_{sat} = \frac{4}{3}[(1 + k)^3/6k]^{1/2}$ through a first-order transition.

For higher values of $k (> 0.5)$, a rather peculiar magnetisation process occurs. Starting from a symmetrical moment configuration, the applied field at first progressively closes the angle between the moments. At a critical field b_{TM} (transverse magnetisation), an abrupt jump occurs to a non-symmetric [1 0, 0 1] configuration. This first-order transition gives rise to a transverse component of the magnetisation (feint lines in figure 3(a)), which is rather unusual in such a symmetric system. Further increasing the field rotates the moments slightly towards the field direction, eventually resulting in another first-order transition, this time to saturation. All the critical lines $b(k)$ are drawn in the
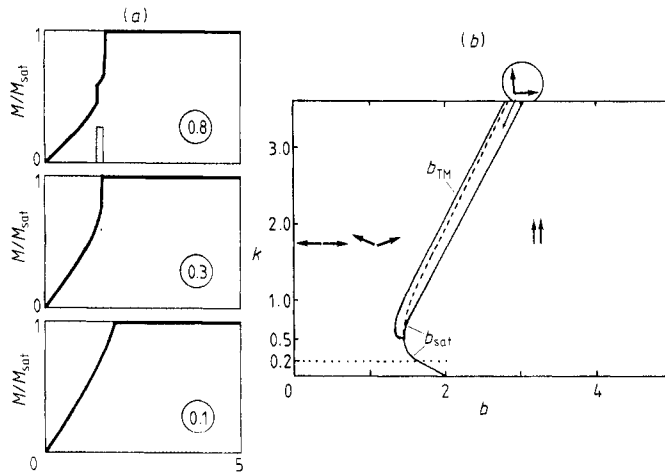

Figure 3. Initial state [0 1, 0 $\bar{1}$]. (a) Three typical magnetisation curves. The feint line in the figure for $k = 0.8$ represents the variation of the transverse magnetisation (i.e. it is non-null between b_{TM} and b_{sat}). (a) Associated phase diagram.

phase diagram of figure 3(b). Lines $b_{TM}(k)$ and $b_{sat}(k)$ for $k > 0.5$ have been determined numerically. The broken line between $b_{TM}(k)$ and $b_{sat}(k)$ is the continuation of the line $b = \frac{4}{3}[(1 + k)^3/6k]^{1/2}$ and corresponds to the saturation field that one would obtain if there was no transition at b_{TM}. Going towards high anisotropy values, this broken line closely approaches b_{TM}. It thus may happen in a real sample that, due to some pinning effects, the b_{TM} transition is 'delayed' and the system may find itself saturated sooner, hence bypassing the intermediate non-symmetric state.

2.2.3. Initial state [1 0, 0 1].

This is the first of the initial states considered that is metastable. The corresponding moment configuration is symmetrical with respect to the hard
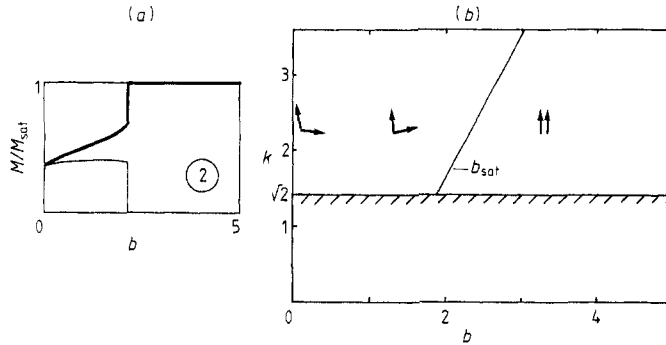
Figure 4. Initial state $[1\,0, 0\,1]$. (*a*) A typical magnetisation curve. The broad line represents the component of the magnetisation parallel to the field while the fine line represents the component perpendicular to the field (the transverse magnetisation). (*b*) Associated phase diagram.

magnetisation direction ([11] direction) and can be stabilised only when $k > \sqrt{2}$, as mentioned previously. Figure 4(*a*) shows examples of longitudinal and transverse magnetisation curves. The magnetisation process is absolutely identical to that of § 2.2.2 after b_{TM}, giving a relatively simple phase diagram with one critical line (figure 4(*b*)). From a practical point of view, the observation of the critical line $b_{sat}(k)$ would be easier for this case than for $[0\,1, 0\,\bar{1}]$ (§ 2.2.2), as the previously mentioned pinning effects would not have a critical influence. One way of initially preparing the system in the $[1\,0, 0\,1]$ state consists of saturating the sample with a field applied along the $[1\,1]$ direction.

2.2.4. Initial state $[\bar{1}\,0, 0\,1]$. The magnetisation process from such an initial state is characterised by two first-order transitions, which delimit a field range of zero magnetisation. The first transition, at a field b_{NA} (non-symmetric/antisymmetric), is a jump to the state $[1\,0, \bar{1}\,0]$ followed by a spin-flip transition (see § 2.2.1), since the anisotropy is required to be $k > \sqrt{2}$. The phase diagram and a typical magnetisation curve are shown in figure 5.

2.2.5. Initial state $[1\,0, 1\,0]$. This case is trivial, the only thing worth mentioning being that the state can exist in zero field only if $k > 1$.
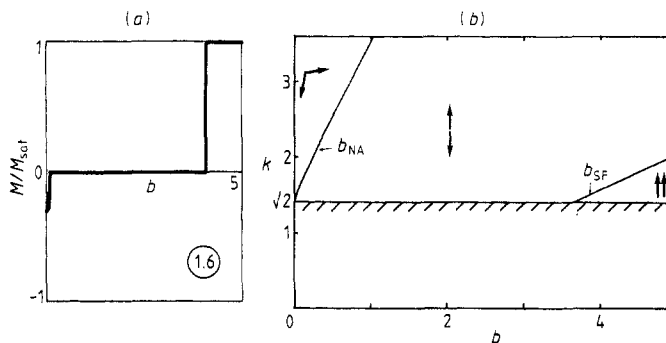

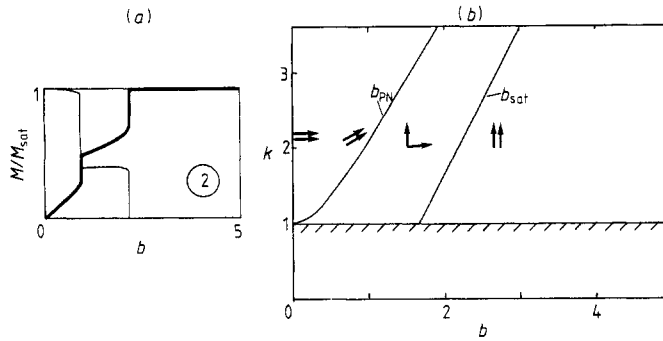**Figure 5.** Initial state $[0\,1, \bar{1}\,0]$. (*a*) Typical magnetisation curve. (*b*) Associated phase diagram.

Figure 6. Initial state $[0\,1,\,0\,1]$. (*a*) Typical magnetisation curve. (*b*) Associated phase diagram.

2.2.6. Initial state $[0\,1,\,0\,1]$. This state is also only stable for $k > 1$ and the magnetisation process is characterised by two first-order transitions (figure 6). The first one at a field b_{PN} (parallel/non-symmetric) is a jump to a non-symmetric $[1\,0,\,0\,1]$ configuration, whereafter the magnetisation process follows that of § 2.2.3.

2.2.7. Initial state $[\bar{1}\,0,\,\bar{1}\,0]$. The same stability condition applies as in § 2.2.6. Depending on k, three types of magnetisation processes may be observed as illustrated in figure 7(*a*). First, if $1 < k < 1.96$, three first-order transitions are observed. In low fields, the magnetisation remains saturated until the field reaches a critical value $b_O = (2k - 1)$, at which the moments jump to the symmetric $[0\,1,\,0\,\bar{1}]$ state. Thereafter the magnetisation follows that of § 2.2.2 with two more first-order transitions.

Over the narrow range $1.96 < k < 2$, the system jumps directly to the non-symmetric state $[1\,0,\,0\,1]$ at b_O and thus only two transitions are observed in the corresponding magnetisation curve. The limiting k-values of this range were determined numerically
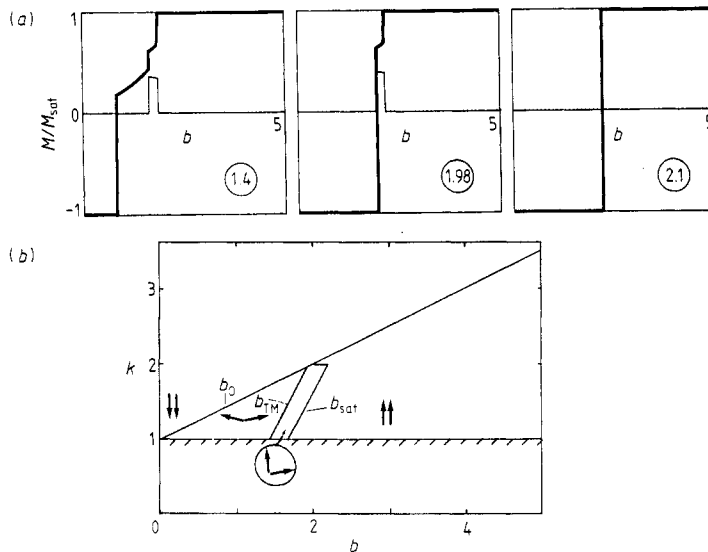

Figure 7. Initial state $[\bar{1}\,0,\,\bar{1}\,0]$. (*a*) Three typical magnetisation curves. (*b*) Associated phase diagram.

by studying the field deformation of the total energy surface by the steepest-descent method. For $k > 2$, the magnetic moments behave like in a switching system, i.e. they jump directly from the $[\bar{1}\,0, \bar{1}\,0]$ to the $[1\,0, 1\,0]$ state and $b_O = b_{sat} = 2(k - 1)$.

2.2.8. Hysteresis loops. In this subsection we discuss the complementary situation to the cases considered in §§ 2.2.1–2.2.7. Starting from a saturated state along an easy magnetisation axis, we examine the demagnetising process when decreasing the field to zero. Typical curves and a phase diagram are shown in figure 8. It is not necessary to consider negative fields further since the remanent state obtained is necessarily one of the initial states of the previous seven subsections.
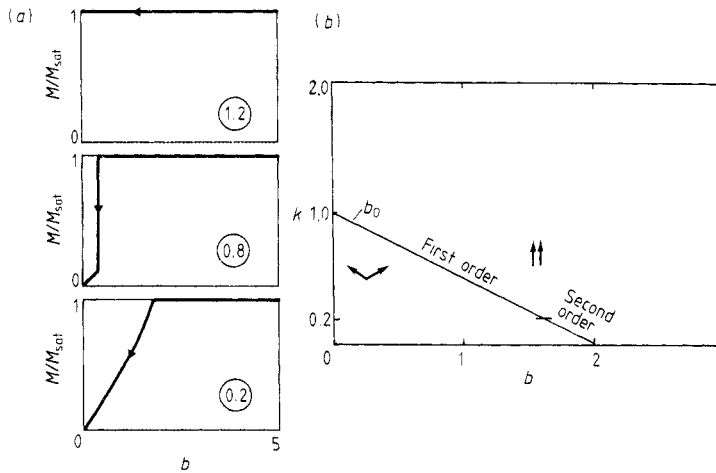
Figure 8. Return from saturation. (*a*) Three typical demagnetisation curves (the demagnetisation occurs in positive fields only if $k < 1$). (*b*) Associated phase diagram. The value $k = 0.2$ separates a second-order departure from saturation from a first-order departure.

Studying the stability of the saturated state shows that the magnetisation remains saturated down to a field $b_O = 2(1 - k)$. Hence, for $k > 1$, the magnetisation remains saturated over the whole range of positive fields and the remanent magnetisation equals the saturation magnetisation. When $k < 1$, departure from saturation occurs in two ways, depending on the strength of the anisotropy.

For $k < 0.2$, as in § 2.2.2, magnetisation reaches saturation by a second-order transition. This is a completely reversible process so that the departure from saturation is also a second-order process with no hysteresis at the transition. The complete cycle is reversible with the two moments always in a symmetric configuration ($\theta_1 = -\theta_2$), reaching $\theta_1 = \pi/2$ in zero field.

For $0.2 < k < 1$, saturation is reached at $b = b_{sat}$ via a first-order process. The departure from saturation occurs at a field value $b_O < b_{sat}$, resulting in some hysteresis. In fields smaller than b_O, the moments are in a symmetric configuration, identical to the situation in § 2.2.2 for increasing fields. Here, also, the remanent magnetisation in zero field is null.

Putting together the results for positive increasing and decreasing fields, five possible hysteresis loop shapes are obtained. They are shown in figure 9. As is usual in antiferromagnetic materials, the shapes have a central symmetry at the origin and consist of
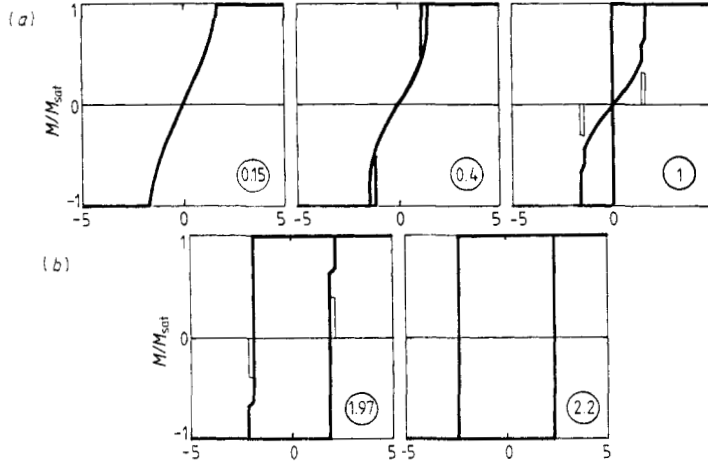
Figure 9. Five typical hysteresis loops. The feint lines indicate the transverse component of the magnetisation.

two subloops shifted symmetrically about the magnetisation axis. As the anisotropy k passes from $k < 1$ to $k > 1$, the remanent magnetisation jumps from zero to saturation. The total energy dissipated per cycle has also been calculated. It is plotted as a function of k in figure 10. The energy is null for $k < 0.2$ and is given by $E = 8(k - 1)$ for $k > 2$, which is the case of a simple switching system. Between these two limiting cases, it increases regularly with positive curvature.
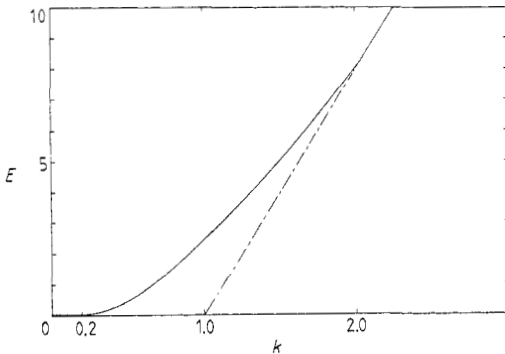
Figure 10. Energy dissipated per cycle versus the anisotropy. The chain line indicates a linear regime reached when the system behaves like a switching dipole ($k > 2$). The equation of this linear regime is $E = 8(k - 1)$.

2.3. $k < 0$

The field in this case is applied along a hard magnetisation axis. In the following six subsections (§§ 2.3.1–2.3.6) the magnetisation/demagnetisation processes and hysteresis loops are investigated as for the $k > 0$ case. The possible initial configurations were sketched in figure 1. Note that, starting from each configuration, the field at which saturation is reached is given by $b_{sat} = 2(1 - k)$ and that this line $b_{sat}(k)$ is the continuation of the line $b_{sat}(k)$ found for $0 < k < 0.2$ in § 2.2.
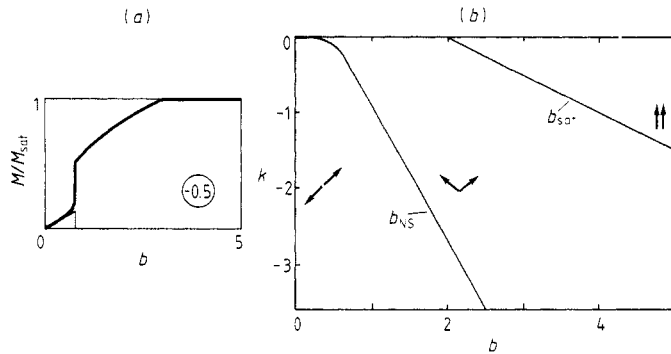
Figure 11. $k < 0$. Initial state $[1\,1, \overline{1}\,\overline{1}]$. (*a*) A typical magnetisation curve. The fine line represents the variation of the transverse component of the magnetisation. (*b*) Associated phase diagram.

2.3.1. Initial state [11, $\overline{1}\,\overline{1}$]. Starting from this configuration, a typical magnetisation curve obtained is shown in figure 11(a). In low fields, small rotations of the moments towards the field direction result in a longitudinal and transverse magnetisation with initially equal susceptibilities (see table 1). This equality is rapidly broken since the initial configuration is not symmetric with respect to the field axis. At a critical field value b_{NS} (non-symmetric/symmetric) a first-order transition occurs corresponding to a jump from the non-symmetric to a symmetric $[1\,\overline{1}, 1\,1]$ configuration. After this transition, the two moments progressively close to the field direction, reaching saturation through a second-order process at $b_{sat} = 2(1 - k)$.

2.3.2. Initial state [1$\overline{1}$, 11]. This state is symmetric with respect to the field and has an initial resultant magnetisation $M_R = [2(1 + 1/k)]^{1/2}$ (recall that each of the moments is assigned unit modulus). The magnetisation curve of figure 12(a) is very regular, with only a second-order transition when reaching saturation.
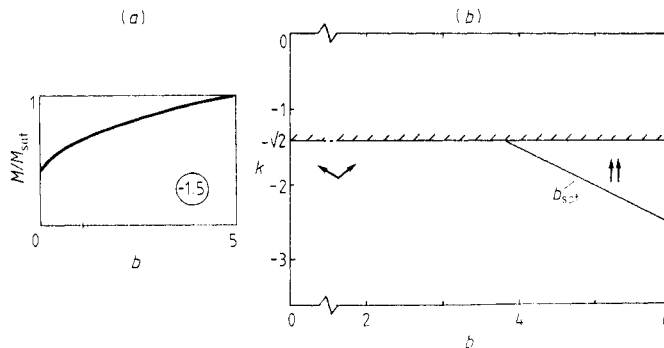

Figure 12. Initial state $[1\,\overline{1}, 1\,1]$. (*a*) A typical magnetisation curve. (*b*) Associated phase diagram.

2.3.3. Initial state [Ī 1, Ī Ī]. A typical magnetisation curve is shown in figure 13(*a*). The configuration remains symmetric in low fields up to b_{SN} where a first-order transition to the non-symmetric [1 1, Ī Ī] state occurs. Hereafter, the magnetisation process follows that of § 2.3.1 with another first-order transition (b_{NS}) followed by a second-order transition at saturation (see figure 13(*b*)).
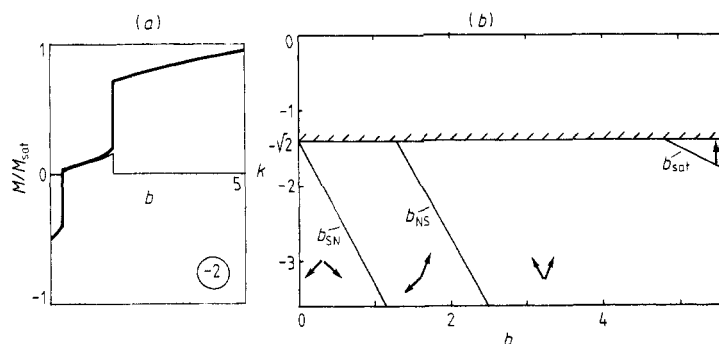

Figure 13. Initial state [Ī 1, Ī Ī]. (*a*) A typical magnetisation curve. (*b*) Associated phase diagram.

2.3.4. Initial state [1 1, Ī 1]. When $k > -3.6$, the magnetisation curve (figure 14(*a*)) exhibits two successive first-order transitions. The first one, at a field b_{NN} (non-symmetric/non-symmetric), corresponds to the jump of one of the moments from the [1 1] state to the [1 Ī] state. The system is then in a nearly antiparallel configuration. A second transition, at a field b'_{NS}, leads to a symmetric [1 1, Ī 1] configuration. When $k < -3.6$, the system does not pass through the intermediate antiparallel phase but directly jumps into the [1 1, Ī 1] configuration. In each case, after the transition to the [1 1, Ī 1] state, saturation is reached at $b_{sat} = 2(1 - k)$ as always. The transition lines are plotted in figure 14(*b*).
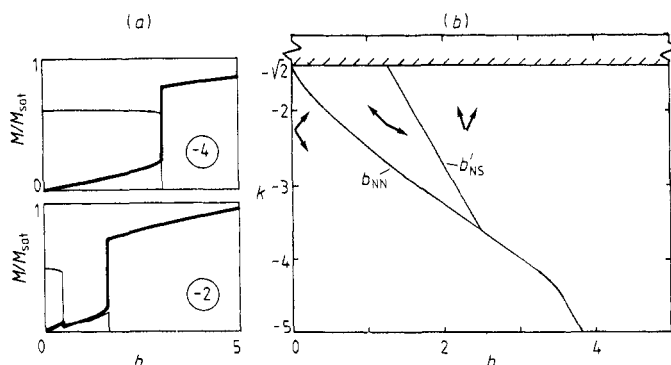

Figure 14. Initial state [1 1, Ī 1]. (*a*) Two typical magnetisation curves. (*b*) Associated phase diagram. The line $b_{sat}(k)$ does not appear in this diagram because it is out of scale.
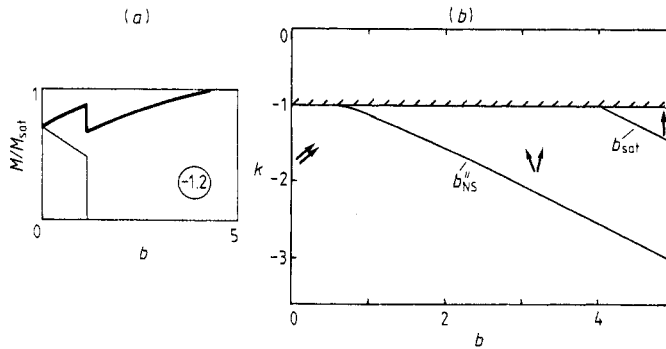
Figure 15. Initial state $[1\,1, 1\,1]$. (*a*) A typical magnetisation curve. (*b*) Associated phase diagram.

2.3.5. Initial state [1 1, 1 1]. Following table 1 the parallel and transverse magnetisations in low fields may be given by $M_{\parallel} = \sqrt{2} - (b/2k)$ and $M_{\perp} = \sqrt{2} + (b/2k)$. The relevant curves and diagram are shown in figure 15. The two moments behave identically ($\theta_1 = \theta_2$) until the field reaches b''_{NS}, at which the system jumps to a symmetric state. Thereafter, the magnetisation process follows that of § 2.3.2.
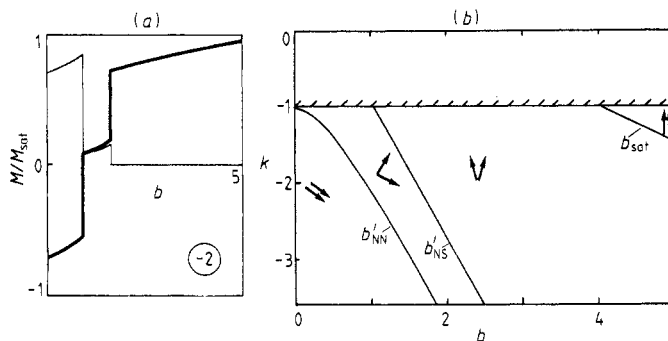

Figure 16. Initial state $[\bar{1}\,1, \bar{1}\,1]$. (*a*) A typical magnetisation curve. (*b*) Associated phase diagram.

2.3.6. Initial state [$\bar{1}$ 1, $\bar{1}$ 1]. In figure 16(*a*), two first-order transitions occur before saturation is reached. The first at b'_{NN} is an irreversible jump between two non-symmetric states ($[\bar{1}\,1, \bar{1}\,1]$ and $[1\,1, \bar{1}\,1]$). As a result, the subsequent magnetisation process follows that of § 2.3.4, giving the phase diagram of figure 16(*b*).

2.3.7. Hysteresis loops. As in § 2.2, it is sufficient to study the demagnetising process in positive decreasing fields from saturation down to zero, in order to derive the complete hysteresis loop (see figures 17(*a*) and (*b*)). The departure from saturation is reversible to a symmetric two-moment configuration. If $k < -\sqrt{2}$ (strong negative anisotropy), there is a positive remanent magnetisation in zero field equal to $[2(1 + 1/k)]^{1/2}$ (table 1). The zero-field configuration is $[1\,\bar{1}, 1\,1]$ (§ 2.3.3). However, if k is between 0 and $-\sqrt{2}$, a transition to a non-symmetric configuration occurs at b'_{SN}. This transition is reversible if $-0.14 < k < 0$ but irreversible for $-\sqrt{2} < k < -0.14$. (The value -0.14 has been
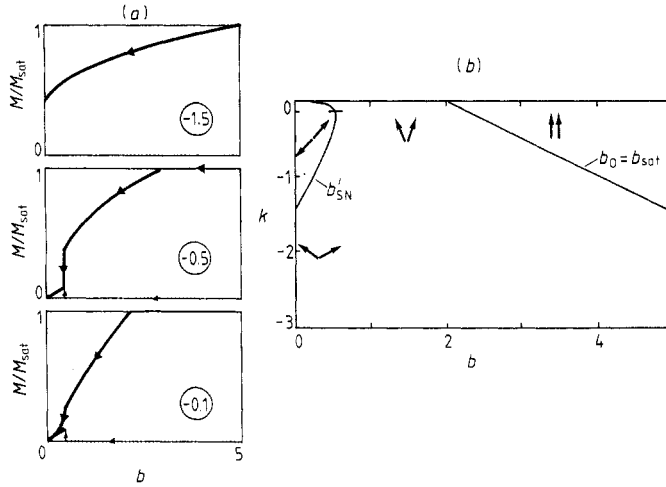
Figure 17. Return from saturation. (*a*) Three typical demagnetisation curves. (*b*) Associated phase diagram.

numerically determined and is the point at which the two curves $b'_{SN}(k)$ and $b_{NS}(k)$ become separate.) For $-\sqrt{2} < k < 0$, therefore, the zero-field state is $[1\,1, \overline{1}\,\overline{1}]$ (§ 2.3.1) with no remanent magnetisation.

At this point one can deduce the possible hysteresis loop shapes, of which there are three, corresponding to the cases $-0.14 < k < 0$, $-\sqrt{2} < k < 0.14$ and $k < -\sqrt{2}$ (see figure 18). The total energy dissipated per cycle has been calculated and is shown in
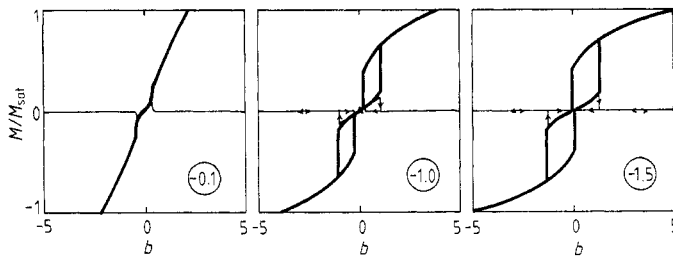

Figure 18. Three typical hysteresis loops. The fine lines indicate the variation of the transverse component of the magnetisation.
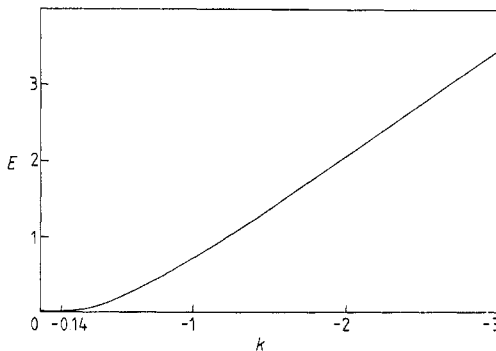

Figure 19. Energy dissipated per cycle versus k in the case of negative anisotropy. This energy is null for $-0.14 < k < 0$.

figure 19. Note that for a given anisotropy the energy dissipated per cycle is much lower when the field is applied along a hard axis of magnetisation (negative anisotropy) than when it is applied along an easy axis of magnetisation (positive anisotropy). It is null for $-0.14 < k < 0$ since the cycle is fully reversible.

3. Magnetisation and demagnetisation processes for uniaxial in-plane anisotropy

The case of uniaxial anisotropy is easier to consider than cubic anisotropy. The anisotropy energy is given by $E_A = -d \cos^2 \theta$, so that the set of equations (3) become

$$- \sin(\theta_1 - \theta_2) + b \sin \theta_1 + d \sin(2\theta_1) = 0$$
$$+ \sin(\theta_1 - \theta_2) + b \sin \theta_2 + d \sin(2\theta_2) = 0$$

(12a)

and

$$- 2\cos(\theta_1 - \theta_2) + b(\cos \theta_1 + \cos \theta_2) + 2d[\cos(2\theta_1) + \cos(2\theta_2)] > 0$$
$$\times [-\cos(\theta_1 - \theta_2) + b \cos \theta_1 + 2d \cos(2\theta_1)]$$
$$\times [-\cos(\theta_1 - \theta_2) + b \cos \theta_2 + 2d \cos(2\theta_2)] - \cos^2(\theta_1 - \theta_2) > 0.$$

(12b)

3.1. $d > 0$

In zero field, there are either one or three possible equilibrium states depending on the strength of the anistropy. Using the notation of § 2, the most stable state is the $[1\,0, \bar{1}\,0]$ configuration. But if $d > 1$, two other states can exist: the $[1\,0, 1\,0]$ and $[\bar{1}\,0, \bar{1}\,0]$ configurations.

3.1.1. Initial state [1 0, $\bar{1}$ 0]. As the field increases, a spin-flop transition is observed at a field $b_{SF} = 2[d(1 + d)]^{1/2}$. The corresponding critical line is drawn in figure 20(b). Note that this expression for $b_{SF}(d)$ is similar to that for $b_{SF}(k)$ in the cubic case. When $d > \frac{1}{3}$, b_{SF} corresponds in fact to a spin-flip transition leading directly to the saturated state. On the other hand, when $d < \frac{1}{3}$, the spin-flop transition leads to a symmetric magnetic state $(\theta_2 = -\theta_1)$ characterised by a constant susceptibility equal to $1/(1 - d)$. Saturation is
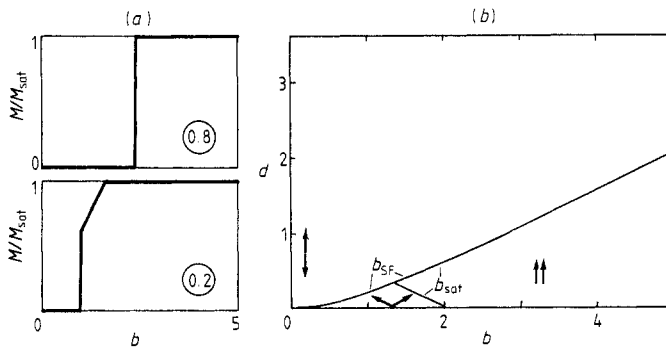

Figure 20. Uniaxial anisotropy. Initial state $[1\,0, \bar{1}\,0]$. (*a*) Two typical magnetisation curves. (*b*) Associated phase diagram.

reached at $b_{sat} = 2(1 - d)$. The two corresponding types of magnetisation curves are illustrated in figure 20(a).

3.1.2. Initial state [1 0, 1 0] ($d > 1$). This case is of little interest since the system is already saturated in zero field and thus remains saturated when the field increases.

3.1.3. Initial state [$\bar{1}$ 0, $\bar{1}$ 0] ($d > 1$). Two magnetisation processes are possible depending on the strength of the anisotropy (see figure 21(a)).

(i) $1 < d < d_c = 1.0756$. Starting from the negative saturated state, a first-order transition occurs at a field b_{SA} (saturated/antiparallel) leading to an antiparallel
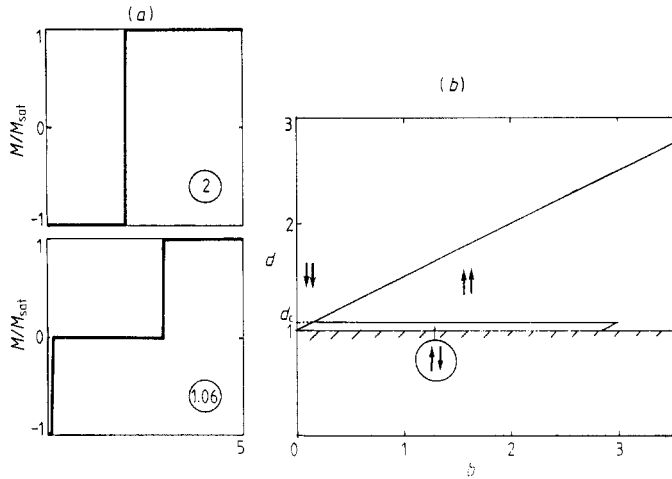

Figure 21. Initial state [$\bar{1}$ 0, $\bar{1}$ 0]. (a) Two typical magnetisation curves. (b) Associated phase diagram.

[1 0, $\bar{1}$ 0] configuration. $b_{SA}(d)$ is given by $b_{SA}(d) = 2(d - 1)$. In higher fields, the magnetic behaviour is identical to the case in § 3.1.1. In particular, saturation is reached through a spin-flip transition.

(ii) $d > 1.0756$. The system behaves like a switching dipole. The total magnetisation reverses abruptly for a field $b_{sat} = 2(d - 1)$.

Note the surprising fact that a small increase of the anisotropy above 1.0756 leads to a large decrease of the saturation field.

3.1.4. Hysteresis loops. At this stage, as in the cubic case, it is sufficient to study the demagnetising processes in positive field in order to derive the entire hysteresis loops.

Starting from saturation and progressively decreasing the magnetic field, saturation remains until $b_O(b_{opening}) = 2(1 - d)$. As a result, the remanent magnetisation is equal to the saturation magnetisation if $d > 1$. But if $d < 1$, a demagnetising process occurs involving a second-order and a first-order transition (see figures 22(a) and (b)). The departure from saturation is a reversible process. The two magnetic moments depart symmetrically from the field axis with the same susceptibility as in increasing fields. An inverse spin-flop transition then occurs at $b_{ISF} = 2(1 - d)[d/(d + 1)]^{1/2}$, leading to the antiferromagnetic state [1 0, $\bar{1}$ 0].
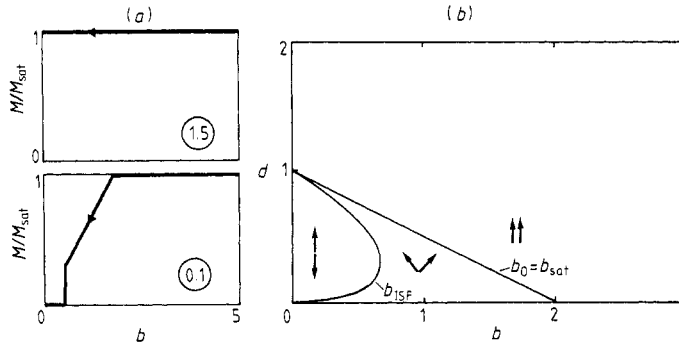
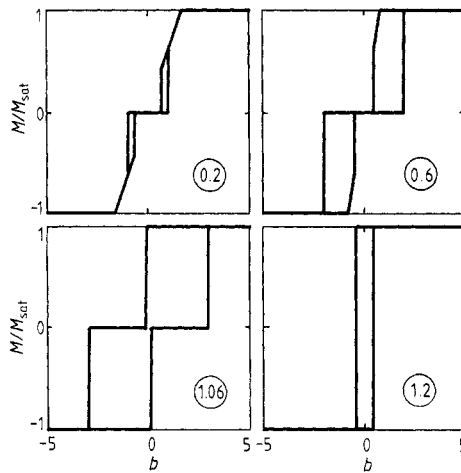**Figure 22.** Return from saturation. (*a*) Two typical demagnetisation curves. (*b*) Associated phase diagram.

Figure 23. Four typical hysteresis loops.

Putting together the results of §§ 3.1.1, 3.1.3 and 3.1.4 gives four types of hysteresis loops ($0 < d < \frac{1}{3}$, $\frac{1}{3} < d < 1$, $1 < d < 1.0756$, $d > 1.0756$). They are illustrated in figure 23.

The total energy dissipated per cycle can be calculated analytically:

if $0 < d < \frac{1}{3}$ $E = 16d^2/(1 - d^2)$

if $\frac{1}{3} < d < 1$ $E = 2\{4[d(1 + d)]^{1/2} - 4(1 - d) + 2(1 - d)/(1 + d)\}$

if $1 < d < 1.0756$ $E = 8\{[d(1 + d)]^{1/2} - (1 - d)\}$

if $d > 1.0756$ $E = 16(d - 1)$.

It is plotted versus d in figure 24. The $E(d)$ curve exhibits a very abrupt jump for the critical value d_c. The origin of this abrupt decrease is that, when $d > d_c$, the system can switch directly from positive to negative saturation, while, when $d < d_c$, it passes through the intermediate antiferromagnetic $[1\,0, \overline{1}\,0]$ configuration and remains pinned in this configuration up to a field b_{SF} much greater than b_O.
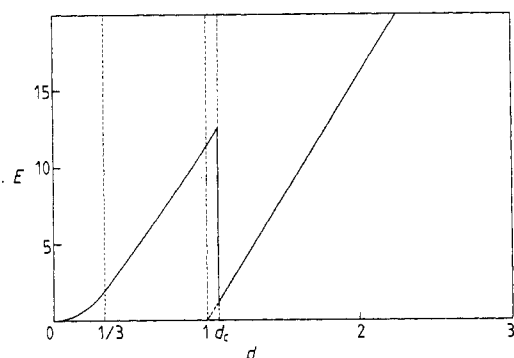
Figure 24. Energy dissipated per cycle for positive uniaxial anisotropy. Note the abrupt decrease for $d = d_c$.

3.2. $d < 0$

In this case, the easy axis of magnetisation lies perpendicularly to the field direction. There are one or two equilibrium initial states possible depending on the strength of the anisotropy. The most stable state is the $[0\,1, 0\,\bar{1}]$ configuration, which exists whatever the value of d. The other one is the $[0\,1, 0\,1]$ configuration, which can be found only if $|d| > 1$.

3.2.1. Initial state $[0\,1, 0\,\bar{1}]$. In this case, the magnetisation process is always reversible (figure 25). The saturation is reached at $b_{sat} = 2(1 - d)$ via a second-order process. Up to saturation, the susceptibility χ is constant and equal to $1/(1 - d)$ as in § 3.1.1 after the spin-flop transition. Note that this is different from the case for cubic anisotropy,
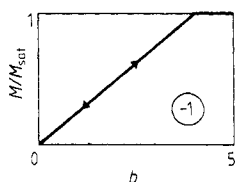

Figure 25. Initial state $[0\,1, 0\,\bar{1}]$. Typical magnetisation curve. This magnetisation process is completely reversible.

where the susceptibility after b_{SF} is not constant but increases as shown by the positive curvature in the magnetisation curves (§ 2).

Since the magnetisation process is completely reversible, no hysteresis is found when cycling the field from positive to negative saturation for $d < 0$.

3.2.2. Initial state $[0\,1, 0\,1]$ $(|d| > 1)$. This initial state can be obtained by previously applying a saturating field in the $[0\,1]$ direction.

A typical magnetisation curve is shown in figure 26(a). It exhibits a first-order transition at a field b_{NS} (non-symmetric/symmetric) corresponding to a jump of the two moments from a non-symmetric transverse configuration $(\theta_1 = \theta_2)$ to a symmetric $(\theta_1 = -\theta_2)$ configuration. Note the interesting fact already observed in §§ 2.2.6 and 2.3.4 that in this kind of transition the magnetisation decreases despite the increasing field. This costs a certain amount of Zeeman energy but is compensated by a decrease of the exchange energy. For $b < b_{NS}$, the longitudinal susceptibility is constant, equal to $1/|d|$, while the transverse susceptibility is initially equal to zero. b_{NS} has the same
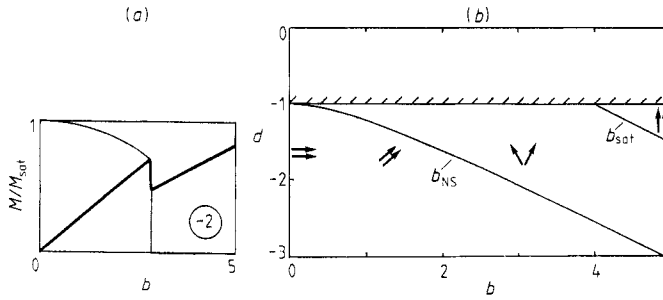
Figure 26. Initial state [0 1. 0 1]. (*a*) A typical magnetisation curve. The feint line represents the variation of the transverse component of the magnetisation. (*b*) Associated phase diagram.

expression as the spin-flop field of § 3.1.1: $b_{NS} = 2[d(d + 1)]^{1/2}$. The curve $b_{NS}(d)$ is drawn in figure 26(*b*). After this first-order transition, the magnetic behaviour is identical to the case in § 3.2.1.

4. Boundary effects

The purpose of this section is to show some of the consequences that a change in the number of layers has on the magnetic behaviour of our model system. We first make a general comparison between a bilayer and an infinite multilayer system. This is followed by an illustrative example for cubic anisotropy of the strong dependence on the number of layers n of the hysteresis loop shape. Then we investigate the influence of n on b_O (departure from saturation) and on b_{SF} (spin-flop/spin-flip) for uniaxial anisotropy.

4.1. Comparison of the magnetic behaviour of a bilayer and a multilayer with no boundaries

In §§ 2 and 3, the magnetic behaviour of a bilayer was investigated. Let us now consider a multilayer consisting of a very large number of layers. In such a system another assumption may be made, which consists of neglecting the boundary effects and assuming that all the layers labelled by an odd (even) index behave in an identical way. This is the usual hypothesis in a mean-field study of bulk antiferromagnets. Hence, the system can be described using simply two moment vectors M_1 and M_2.

Assuming $\theta_1 = \theta_3 = \ldots = \theta_{2p+1}$ and $\theta_2 = \theta_4 = \ldots = \theta_{2p}$, the set of equations (2) (§ 1) reduce to

$$- J \sin(\theta_1 - \theta_2) + B \sin \theta_1 + \partial E_{A1}/\partial \theta_1 = 0$$

$$- J \sin(\theta_2 - \theta_1) + B \sin \theta_2 + \partial E_{A2}/\partial \theta_2 = 0$$

where $J = 2J_0$. This set of equations is exactly the same as that of a 'true bilayer' (equations (3)) but with an interaction $2J_0$ instead of J_0. So, if the two-layer description is correct, the magnetic behaviour (magnetisation curves, phase diagram, . . .) of the infinite multilayer and bilayer should be exactly the same provided that the field and anisotropy are normalised to the effective coupling strength ($2J_0$ or J_0). This permits

magnetic behaviour for $n = \infty$ to be deduced from the $n = 2$ case using the scaling laws

if $M(n = 2) = f(B/J_0, D/J_0)$ then $M(n = \infty) = f(B/2J_0, D/2J_0)$

and for the transition fields

if $B_{\text{trans}}(n = 2)/J_0 = g(D/J_0)$ then $B_{\text{trans}}(n = \infty)/J_0 = 2g(D/2J_0)$.

In the next section, we study the influence of the number of layers on the shape of the hysteresis loop in a particular case of cubic anisotropy. The two following sections are devoted to analytical calculations of the dependence on n of two typical transition fields. The comparison of the cases $n = 2$ and $n \to \infty$ will illustrate the validity and/or limits of the two-layer descriptions of an infinite multilayer.
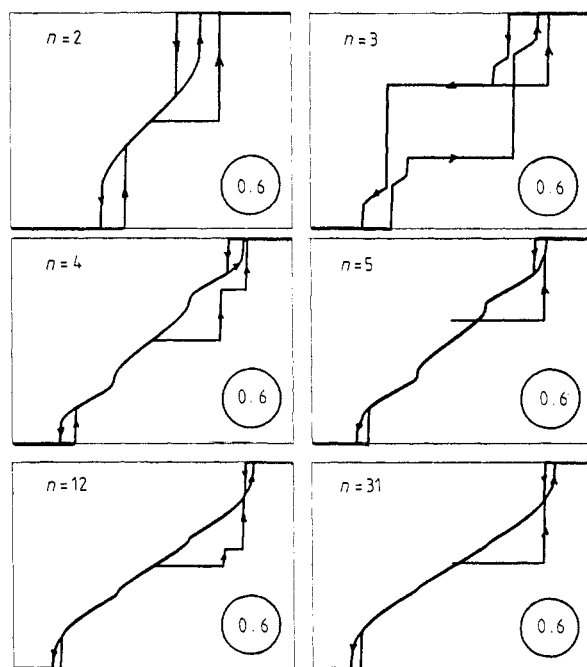

Figure 27. Initial magnetisation curves and hysteresis loops obtained in the case of cubic anisotropy with $k = 0.6$ for six different values of the number of layers: $n = 2, 3, 4, 5, 12, 31$.

4.2. The n dependence of the shape of the hysteresis loops in the particular case of cubic anisotropy with $K/J_0 = 0.6$

The magnetisation of the multilayer is here described by n variables $\theta_1, \theta_2, \ldots, \theta_n$ and the total energy is minimised using the steepest-descent method described in § 1. In all the calculations, the initial configuration in zero field is given by $\theta_1 = \theta_3 = \ldots = \theta_{2p+1} = 0$ and $\theta_2 = \theta_4 = \ldots = \theta_{2p} = \pi$. The resulting initial magnetisation curves and hysteresis loops are shown in figure 27 for six values of n. These results require some comment.

(i) A great difference exists between the cases $n = 2$ and $n = 3$. The principal origin of this difference is that for an odd number of layers the magnetisation is not compensated

in zero field while it is for n even. As a result, another loop appears in the hysteresis cycle for $n = 3$, which is centred on the origin, while the others are shifted symmetrically along the field axis. This central loop is similar to that observed in bulk ferrimagnetic materials. It disappears for $n \geq 5$ because the demagnetising process for higher values of n leads to a configuration in zero field characterised by a transverse direction of antiferromagnetism $(\theta_{2p} = \pi/2, \theta_{2p+1} = -\pi/2)$, while it leads to a configuration characterised by a parallel direction of antiferromagnetism $(\theta_{2p} = \pi, \theta_{2p+1} = 0)$ for $n = 3$.

(ii) As the number of layers increases, the general shape of the hysteresis loop becomes smoother and, for this value of the anisotropy, it tends towards the same shape as in the case $n = 2$, with of course different transition fields. Quantitatively, we have verified that the initial magnetisation curve and hysteresis loop of a bilayer with an anisotropy constant $K/J_0 = k = 0.3$ is very close to that obtained here for $n = 31$ with a simple scale factor of 2 for the field. This means that in this particular case the 'two-layer description' of this multilayer with $n = 31$ is valid.

4.3. The n dependence of b_O

Let us now consider a multilayer consisting of n layers with uniaxial anisotropy. The field is applied along the easy axis of magnetisation.

Starting in high fields from a saturated state and decreasing the field progressively, at a field b_O the saturated state becomes unstable and the magnetisation begins to decrease. In order to calculate $b_O(n, d)$, we form the matrix M_n given by

$$M_{ij} = \left(\frac{\partial^2 E_n}{\partial \theta_i \partial \theta_j} \right).$$

The value b_O is obtained when one of the eigenvalues of this matrix reaches zero, i.e. when $\det M_n = 0$. The form of $\det M_n$ is deduced for the saturated state from the total energy expressed in units of J_0:

$$E_n = [\cos(\theta_1 - \theta_2) + \cos(\theta_2 - \theta_3) + \ldots + \cos(\theta_{n-1} - \theta_n)] - b(\cos \theta_1$$
$$+ \cos \theta_2 + \ldots + \cos \theta_n) - d(\cos^2 \theta_1 + \cos^2 \theta_2 + \ldots + \cos^2 \theta_n).$$

Letting $u = -1 + b + 2d$ and $v = -2 + b + 2d$ $(=u - 1)$ then

$$\det M_n = \begin{vmatrix} u & 1 & & 0 & \cdots & \cdots & 0 \\ 1 & v & 1 & & & & \\ 0 & 1 & v & & & & \\ & & & \ddots & & 1 & 0 \\ & & & & 1 & v & 1 \\ 0 & \cdots & \cdots & 0 & 1 & u \end{vmatrix}. \tag{13}$$

Introducing α, where $v = 2 \cos \alpha$, $\det M_n$ can be calculated as

$$\det M_n = u^2 \frac{\sin[(n-1)\alpha]}{\sin \alpha} - 2u \frac{\sin[(n-2)\alpha]}{\sin \alpha} + \frac{\sin[(n-3)\alpha]}{\sin \alpha}. \tag{14}$$
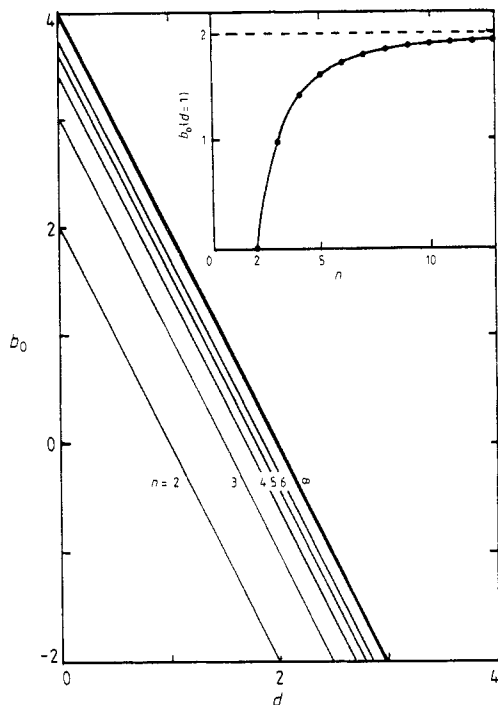
Figure 28. b_O (field for which the departure from saturation occurs) in the case of a uniaxial anisotropy versus the strength of the anisotropy d for various numbers of layers. Inset: for the particular value $d = 1$, variation of b_O versus n.
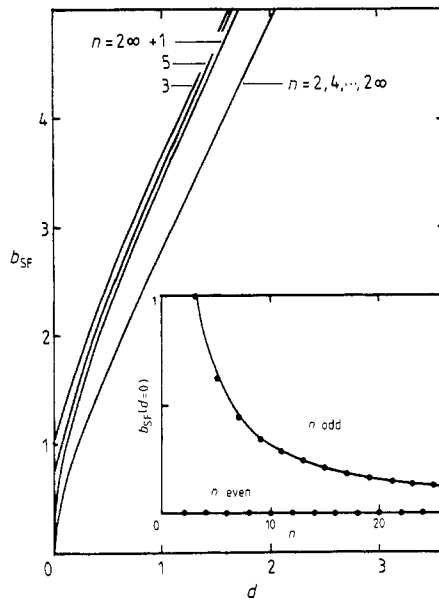
Figure 29. b_{SF} (spin-flop transition) versus d for various numbers of layers. Inset: for the particular value $d = 0$, variation of b_{SF} versus n. The full line is a fit of $b_{SF}(n)$ for n odd and is given by the equation $b_{SF}(n) = 3.136/n$.

Therefore the condition that det $M_n = 0$ is equivalent to

$$v = 2 \cos \alpha$$

$$(v + 1) \sin[(n - 1)\alpha] - 2(v + 1) \sin[(n - 2)\alpha] + \sin[(n - 3)\alpha] = 0. \quad (15)$$

Each value of n gives a solution (α_n^0, v_n^0), so that $b_O(n, d)$ is given by

$$b_O(n, d) = 2 + v_n^0 - 2d. \quad (16)$$

This formula shows that $b_O(n, d)$ has a linear dependence on d with the same slope as calculated in § 3 for $n = 2$. $b_O(n, d)$ is plotted in figure 28 for various values of n. As $n \to \infty$, equations (15) give $\alpha \to 0$ and $v \to 2$, so that $b_O(\infty, d) = 4 - 2d$. This may be written as $b_O(\infty, d)/2 = 2 - 2 \times d/2$ to be compared with $b_O(2, d) = 2 - 2 \times d$ found in § 3. This comparison shows that the scaling relations of § 4.1 work well for the present case.

4.4. The n dependence of b_{SF}

Here we consider the same multilayers as in the previous section but we start from an initial antiferromagnetic configuration ($\theta_1 = \theta_3 = \ldots = \theta_{2p+1} = 0; \theta_2 = \theta_4 = \ldots = \theta_{2p} = \pi$) and progressively increase the applied field. At b_{SF} the system jumps either to

a symmetric $(\theta_1 = -\theta_2 = \ldots = \theta_{2p+1} = -\theta_{2p})$ configuration or to saturation if the anisotropy is large. Using the same method as in the previous case, we introduce $w = 1 + b + 2d, x = 1 - b + 2d, y = 2 + b + 2d$ and $z = 2 - b + 2d$. Depending on the parity of the number of layers n, two expressions for $\det M_n$ are possible: if n is even

$$\det M_n = \begin{vmatrix} w & -1 & 0 & & & & & & 0 \\ -1 & z & -1 & & & & & & \\ 0 & -1 & y & -1 & & & & & \\ & & -1 & z-1 & & & & & \\ & & & -1 & y & -1 & & & \\ & & & & -1 & z & -1 & & \\ & & & & & -1 & y & -1 & \\ 0 & & & & & & 0 & -1 & x \end{vmatrix}$$

and if n is odd

$$\det M_n = \begin{vmatrix} w & -1 & 0 & & & & & & 0 \\ -1 & z & -1 & & & & & & \\ 0 & -1 & y & -1 & & & & & \\ & & -1 & z & -1 & & & & \\ & & & -1 & y & -1 & & & \\ & & & & -1 & y & -1 & & \\ & & & & & -1 & y & -1 & 0 \\ & & & & & & -1 & z & -1 \\ 0 & & & & & & 0 & -1 & w \end{vmatrix} . \qquad (17)$$

For each value of the anisotropy d, the spin-flop field $b_{SF}(n, d)$ is the smallest solution of the equation $\det M_n = 0$. For $n = 2$, we found (§ 3) $b_{SF}(2, d) = 2(d^2 + d)^{1/2}$ and for $n = 3, b_{SF}(3, d) = \{1 + [1 + 4(6d + 4d^2)]^{1/2}\}/2$. The critical lines $b_{SF}(n, d)$ are plotted in figure 29.

Several interesting points arise from this analysis. Clearly, two sets of curves are obtained for b_{SF} depending on the parity of n. If n is even, all the curves $b_{SF}(n,d)$ are identical to $b_{SF}(2, d) = 2(d^2 + d)^{1/2}$, i.e. the spin-flop field is independent of the number of layers. (This is also true in the case of a cubic anisotropy—see figure 27 for n even.) On the contrary, if n is odd, distinct curves are obtained which tend towards a limiting curve as n increases. The equation of this limiting curve is $b_{SF}(2 \infty +1, d) = 2(d^2 + 2d)^{1/2}$. Hence, the spin-flop field obtained with an odd number of layers is greater than that obtained with an even number. The physical reason for this is that, for an odd value of n, the magnetisation of the multilayer is not compensated.

A spontaneous moment exists in low fields, parallel to the field, and this tends to stabilise the antiferromagnetic configuration. As a result, a stronger field is needed to provoke the spin-flop transition. Concerning the limit of an infinite number of layers, these results are rather surprising, i.e. in the limit of infinite n, depending on the parity of n, there are two different expressions for b_{SF}: $b_{SF}(2\infty, d) = 2(d^2 + d)^{1/2}$ and $b_{SF}(2\infty + 1, d) = 2(d^2 + 2d)^{1/2}$. Note furthermore that the second expression fulfils the scaling relation of § 4.1, i.e.

$$b_{SF}(2\infty + 1, d)/2 = 2[(d/2)^2 + (d/2)]^{1/2} = b_{SF}(2, d/2)$$

but not the first.

In other words, this means that the boundary effects disappear when n tends to infinity if n is odd but not so if n is even. Physically this can be explained by the fact that when n is even the two moments at the extremity of the chain are antiparallel. The one that is opposed to the field plays a crucial role in the spin-flop transition since it has only one neighbour and thus may act as a lever in order to flip up all the chain. It is for this reason that, even with an infinite chain, the boundary effects remain relevant in the even-n case. On the contrary, in the odd-n case, the two extreme moments are parallel to the field. All the moments oriented antiparallel to the field have two neighbours so that in this case the boundary effects disappear.

It is therefore clear that the number of layers can play an important role in the magnetisation process of a multilayer system. In particular, it is important to know whether or not the total magnetisation is compensated.

5. Conclusions

We have studied magnetisation and demagnetisation processes in highly idealised multi-layer systems consisting of ferromagnetic layers of uniaxial or cubic anisotropy with antiferromagnetic coupling between adjacent layers. In the case of a bilayer, for both anisotropy symmetries, the magnetic phase diagrams were fully investigated for the various initial moment configurations and all the critical lines defining first- and second-order transitions have been reported. Typical magnetisation curves have also been shown, to illustrate the different magnetisation processes. It was subsequently possible to deduce the different hysteresis loop shapes for each of the symmetries, and these too have been reported. In the cubic case, which is more complex than the uniaxial case, apart from spin-flop and spin-flip transitions, several first-order transitions between symmetric and non-symmetric states were calculated, giving rise to quite complicated magnetisation processes and phase diagrams. Size and boundary effects were also examined in § 4. It was shown that in most cases simple scaling relations exist to deduce the magnetic behaviour of an infinite multilayer from that of a simple bilayer. The dependence of the departure from saturation field b_O on the number of layers n was calculated and was found to satisfy the scaling relations when $n \to \infty$. The spin-flop (spin-flip) field b_{SF}, however, does not fully satisfy these relations since the boundary effects may play an important role even if the number of layers tend to infinity. In a following paper, we shall study in more detail the influence of the number of layers on the magnetisation processes.

These calculations of magnetisation processes also apply to bulk materials that consist of antiferromagnetically coupled ferromagnetic atomic layers when the moments are confined within individual planes.

The model used could be improved by introducing longer-range interactions between layers [13, 14] or by taking into account the non-infinite rigidity of the magnetisation of the ferromagnetic films [15]. Furthermore, we should consider the second limiting situation, which consists of assuming that, by nucleation and propagation of domain walls, the system can always reach the state of absolute minimum energy [16]. In a real sample, the magnetisation process will be a more or less complicated intermediary between those calculated for these two limiting cases. Nevertheless, the present study already identifies some general tendencies and reveals different kinds of transitions that may be observed, at least partially, in a real sample.

Acknowledgments

References

[1] Chang L L and Giessen B C (ed.) 1985 *Synthetic Modulated Structures* (New York: Academic)
[2] Salamon M B, Sinha S, Rhyne J J, Cunningham J E, Erwon R, Borchers J and Flynn C P 1986 *Phys. Rev. Lett.* **56** 259
[3] Majkrzack C F, Cable J W, Kwo J, Hong M, McWhan D B, Yafet Y, Waszizak J V and Vettier C 1986 *Phys. Rev. Lett.* **56** 2700
[4] Schuller I K 1988 *Physics, Fabrication and Applications of Multilayered Structures* ed. P Dhez and C Weisbuch (Berlin: Springer)
[5] Khan M R, Roach P and Schuller I K 1984 *Thin Solid Films* **122** 183
[6] Hosoito N, Kawaguchi K, Shinjo T, Takada T and Endoh Y 1984 *J. Phys. Soc. Japan* **53** 2659; Wong H K 1985 *PhD Thesis* Northwestern University, Evanston
[7] Herman F, Lambin P and Jepsen O 1985 *Phys. Rev.* B **31** 4394
[8] Grunberg P 1985 *J. Appl. Phys.* **57** 3673
[9] Erwin R W, Rhyne J J, Salamon M B, Borchers J, Sinha S, Du R, Cunningham J E and Flynn C P 1987 *Phys. Rev.* B **35** 6808
[10] Nguyen Van Dau F, Fert A, Etienne P, Baibich M N, Broto J M, Chazelas J, Creuzet G, Friederich A, Hadjoudj S, Hurdequint H, Redoules J P and Massies J 1988 *J. Physique Coll.* **49** (C8) 1633
[11] Cebollada A, Martinez J L, Gallego J M, Wiranda R, Ferrer S, Batallan F, Fillion G and Rebouillat J P 1989 *Phys. Rev.* B *Rapid Commun.* **39** 9726
[12] Grunberg P, Schreiber R, Pang Y, Brodsky M B and Sowers H 1986 *Phys. Rev. Lett.* **57** 2442; Grunberg P 1988 *Proc. 12th ICMFS, Le Creusot, 1–5 Aug*
[13] Rossat-Mignod J, Burlet P, Villain J, Bartholin H, Tcheng-Si W, Florence D and Vogt O 1977 *Phys. Rev.* B **16** 440
[14] Yamashita M, Kurisu M, Kadomatsu H, Oguro I and Fujiwara H 1987 *J. Phys. Soc. Japan* **56** 32
[15] Nguyen Van Dau F 1989 *PhD Thesis* Orsay
[16] Dieny B and Gavigan J P 1990 *J. Phys.: Condens. Matter* **2** 187–94